Astronomy & Astrophysics manuscript no. aa61347-26
July 22, 2026
©ESO 2026

Letter to the Editor

Molecular gas hidden in plain sight in the early Universe

Pasquier Noterdaeme[1], Jens-Kristian Krogager[2,3], and Sergei Balashev[4]

[1] Institut d'Astrophysique de Paris, CNRS-SU, UMR 7095, 98bis bd Arago, 75014 Paris, France – e-mail: noterdaeme@iap.fr
[2] French-Chilean Laboratory for Astronomy, IRL 3386, CNRS and U. de Chile, Casilla 36-D, Santiago, Chile
[3] Université Lyon 1, ENS de Lyon, CNRS, CRAL, UMR 5574, Saint-Genis-Laval, France
[4] Ioffe Institute, Polyteknicheskaya 26, 194021 Saint-Petersburg, Russia

July 22, 2026

ABSTRACT

We report the discovery of an extreme intervening molecular absorber at $z_{\rm abs} = 4.1$ towards the $z = 4.7$ quasar SDSS J080023.02+305101.22 revealed through strong H_2 absorption that had remained unnoticed in archival data for about two decades. The system, which we analysed with new VLT/X-shooter observations, has a metallicity of about one-fifth the solar value, in line with the moderate dust reddening $A_V \sim 0.06$ mag. More strikingly, it exhibits the highest molecular fraction, $f_{\rm H_2} = 2N({\rm H_2})/(2N({\rm H_2}) + N({\rm H\,I})) \approx 60\,\%$, measured at $z > 0$ from direct determinations of both atomic and molecular hydrogen column densities. Notably, this fraction is comparable to the very highest values in the Local Group. The inferred $f_{\rm H_2}$ still represents a conservative lower limit to the local molecular fraction since the H I absorption very likely includes atomic gas unrelated to the actual molecular component, as indicated by the wide ($\Delta v \sim 500$ km s^{-1}) multi-component low-ionisation metal profile.
The detection of such a system at early cosmic times is remarkable given the limited number of quasar spectra probing $z > 4$. It suggests an unexpectedly high incidence of H_2, with important implications for the evolution of molecular gas. This high incidence may be driven by high average densities and enhanced turbulence at those redshifts. At the same time, our results also highlight possible observational biases, both in quasar selection and in recognising strong H_2 absorption, suggesting that a significant fraction of molecular gas may remain undetected, in particular near the peak of star formation.
The present system offers a unique benchmark for developing efficient detection algorithms. Further progress will benefit from colour-independent quasar surveys, while constraining the physical conditions and environments of such extreme absorbers will require observations on future extremely large telescopes.

Key words. Quasars: absorption lines – ISM: molecules

arXiv:2607.18974v1 [astro-ph.GA] 21 Jul 2026

1. Introduction

The central role of molecular gas in galaxy evolution is no longer in question, as it constitutes the immediate fuel for star formation. What remains less constrained, however, is where and under which conditions the bulk of molecular gas resides, especially at high redshift. In fact, the dominant constituent of molecular gas, H_2, is notoriously difficult to detect in emission, so indirect tracers such as CO are widely used instead. While absorption spectroscopy provides a direct, distance-insensitive probe of H_2 through the electronic Lyman and Werner bands, the small cross-section of cold, dense molecular clouds implies that intercepting such gas beyond the Local Group along random sightlines, i.e. at $z > 0$ towards quasars, is intrinsically rare.

Despite its fundamental importance and significant observational progress (Balashev & Noterdaeme 2018, based on average H_2 absorption signal), the column-density distribution of H_2 remains poorly constrained at its high end. The most molecular-rich absorption systems are not only intrinsically the rarest, but they are also suspected to be systematically missed: H_2 absorbers are commonly associated with dust reddening of the background quasar, particularly at high metallicity (e.g. Noterdaeme et al. 2017; Balashev et al. 2019). At high column densities, the many H_2 lines also blend together and absorb most of the far-UV flux (Noterdaeme et al. 2015). As a result, in addition to strengthening potential biases in the quasar photometric selection (Fall & Pei 1993; Krogager & Noterdaeme 2020), the strongest H_2 systems could in fact also be difficult to recognise in the quasar spectra, especially at high redshift, where the overall transmission of the intergalactic medium is already low.

Here we report the discovery of an extreme intervening H_2 absorber associated with the $z = 4.096$ damped Ly-α system (DLA) towards the bright $z = 4.67$ quasar SDSS J080023.02+305101.22 (hereafter J 0800+3051). This is only the third H_2 absorption system detected at $z > 4$ (Ledoux et al. 2006b; Noterdaeme et al. 2026), but, most importantly, it has the highest molecular fraction directly measured (i.e. from H_2 and H I lines) at $z > 0$. Finally, and somewhat paradoxically, this quasar and the intervening DLA have been known for about two decades, but the strong H_2 system remained unrecognised until now. We present data of J 0800+3051 from different surveys in Sect. 2 along with new observations collected with the X-Shooter spectrograph on the Very Large Telescope (VLT) of the European Southern Observatory (ESO). We present our analysis and properties of the system in Sect. 3 and discuss our results and conclude in Sect. 4.

2. Survey data and new observations

2.1. Public survey data

The object J 0800+3051 was first targeted for spectroscopic observations in early 2003 by the Sloan Digital Sky Survey (SDSS; York et al. 2000, with resolution power of $R \sim 2000$) as a

high-redshift quasar candidate (Richards et al. 2002). Its formal identification as a quasar was then reported by Schneider et al. (2005) based on this spectrum. Prochaska et al. (2005) subsequently detected the $z = 4.1$ DLA using an automated procedure followed by visual inspection and fit of the H I line, reporting $\log N(\mathrm{H\,I})/\mathrm{cm}^{-2} = 20.8$. The quasar was re-observed by the SDSS-III in 2010 in the course of the Baryon Oscillation Spectroscopic Survey (Dawson et al. 2013).

The high redshift and luminosity of the quasar motivated several follow-up studies, both to characterise the quasar itself (e.g. Trakhtenbrot et al. 2011) and to investigate intervening diffuse gas at early cosmic times. The aim of the Giant Gemini GMOS survey (Worseck et al. 2014, with $R \sim 900$ but high S/N) was to constrain the mean free path of ionising photons at high redshift and identify DLAs (Crighton et al. 2015) as well as Lyman-limit systems (Crighton et al. 2019), the latter based on the detection of sharp flux discontinuities bluewards of the Lyman limit. These studies also involved visual inspections of the quasar spectrum, including focusing on the DLA, but they did not report the presence of strong molecular absorption. Finally, this system did not pass the threshold confidence cuts in the first automated search for H_2 absorption in DLAs either (Balashev et al. 2014).

2.2. New observations: VLT/X-shooter and 4MOST

Following a serendipitous identification of the system, we observed J 0800+3051 twice with X-shooter (Vernet et al. 2011) through Director's Discretionary Time on January 25, 2026, under Prog ID 116.2AQ1 (PI Noterdaeme). Each observation consisted of a $\sim$ 3000 s exposure for the UVB and VIS arms and 5×600 s exposures for the near-infrared, with slit widths of respectively 1.0, 0.9, and 0.9". The observations were performed in dark time under good conditions (clear sky with 0.7" seeing), though at relatively high airmasses (1.7-2) given the high declination of the target. The airmass-corrected seeing being slightly larger than the slit widths, the nominal spectral resolutions were obtained with $R = 5400$, 8900, and 5600 for the UVB, VIS, and near-infrared, respectively. The data were reduced using the ESO pipeline v3.5.3 to produce the 1D spectra for each arm, which we combined using an inverse-variance weighting. Absorption from the Earth's atmosphere was modelled for each exposure using Molecfit (Smette et al. 2015), and the corresponding transmissions were combined in the same way as the science data to produce an effective atmospheric transmission model.

The quasar was also serendipitously observed for 1 hour during commissioning of 4MOST (de Jong et al. 2019) in December 2025 in order to check the effectiveness of observations at high airmass and test the performance of the redshift pipeline. The 4MOST data, covering 3700 to 9500 Å at $R \approx 5000$, were processed using the official pipeline v0.9 (from date December 22, 2025), with daytime calibrations obtained the morning after.

3. Properties of the molecular absorption system

The overall spectral shape of J 0800+3051 appears to be typical of quasars (Fig. 1). By matching the X-shooter data with the composite spectrum of Selsing et al. (2016), shifted to the same emission redshift and reddened assuming a Small Magellanic Cloud type extinction law (Gordon et al. 2003) at $z = 4.1$, we inferred a moderate amount of dust in the DLA, with $A_V \sim 0.06$ mag[1]. In turn, bluewards of the quasar Ly-α emission, a very significant drop in transmission was observed. This results from the mutual blending of H_2 lines in the DLA, as shown in the inset panel, together with unrelated intervening H I absorption.

Simultaneous multiple Voigt-profile fitting was then used to derive column densities (N), Doppler parameters (b), and redshifts (z) of the atomic and molecular absorption lines at $z = 4.1$, including the effective atmospheric transmission in the total absorption model during the fit. Details on the analysis are provided in the Appendix, and we briefly summarise the obtained measurements here.

Molecular hydrogen lines were detected across many rotational levels, with consistent features up to $J = 9$ (see Figs. 1 and A.4). The column density was well constrained for the lowest rotational levels ($J < 4$), which contain the bulk of H_2 and produce strongly damped lines. Furthermore, the damped lines are insensitive to the Doppler parameter and the velocity structure and are thus reasonably well constrained. From their excitation, we inferred a kinetic temperature of $T_k \approx T_{01} = 97^{+15}_{-12}$ K. Measuring the H_2 column densities in higher J-levels was very challenging due to the line blending (see Appendix), impeding their use to constrain the physical conditions.

From the metal and hydrogen column densities ($\log N(\mathrm{H\,I}) = 20.8 \pm 0.1$; $\log N(H_2) = 20.66 \pm 0.04$) in the system, we inferred an average gas-phase metal abundance of [Si/H] ≈ -0.7. This metallicity is consistent with that expected from the ~ 500 km s^{-1} wide velocity profile according to the metallicity–velocity relation observed by Ledoux et al. (2006a). The overall molecular fraction was found to be $f_{H_2} = 2N(H_2)/(2N(H_2) + N(\mathrm{H\,I})) = 0.59 \pm 0.08$. This is a very conservative lower limit to the actual value in the H_2-bearing cloud since the observed $N(\mathrm{H\,I})$ includes the many components seen in the metal-line profile. Assuming the overall metallicity is representative of that in the H_2-bearing component, we inferred a more realistic value of $f \approx 0.9$ at $v = 0$ km s^{-1}, which is still conservative. Indeed, H_2 is expected to arise in the regions with the highest metallicity due to its formation on the surface of dust grains. Furthermore, H I-H_2 transition models (Bialy & Sternberg 2016) predict that beyond the dissociation front, the gas becomes fully molecular, with the observed H I arising from the cloud's outer envelope. Following these transition models, the observed H I column density and the moderate dust-to-gas ratio suggest a density-to-UV field ratio typical of cold gas with $n/I_{\mathrm{UV}} > 100\,\mathrm{cm}^{-3}$, where I_{UV} is relative to the Draine (1978) interstellar radiation field (i.e. the mean Lyman-Werner band flux density is given by $\overline{F}_\nu = 2.46 \times 10^{-8} I_{\mathrm{UV}}$ photon cm^{-2} s^{-1} Hz^{-1}).

4. Discussion and conclusions

So far, large molecular hydrogen column densities have been preferentially identified in systems pre-selected for their extreme H I content. Ranjan et al. (2018) reported a very high H_2 column density towards an extremely strong DLA (Noterdaeme et al. 2014), while Balashev et al. (2017) confirmed the presence of strong H_2 absorption previously identified through an automated search from Balashev et al. (2014) applied to the SDSS-III DLA sample (Noterdaeme et al. 2012). In these cases, the associated H I column densities are among the highest known, in line with the scenario proposed by Noterdaeme et al. (2015), in which H_2 is preferentially found in high-pressure environments, possibly located in the inner regions of galaxies. Supporting evidence includes the observed anti-correlation between the H I column density and impact parameter (Krogager et al. 2020), and the statistical detection of Ly-α emission superimposed on strong DLAs (Noterdaeme et al. 2014). We also note the detection of

[1] The systematic uncertainty is comparable to the inferred value, due to intrinsic quasar shape variation; see Noterdaeme et al. (2017).

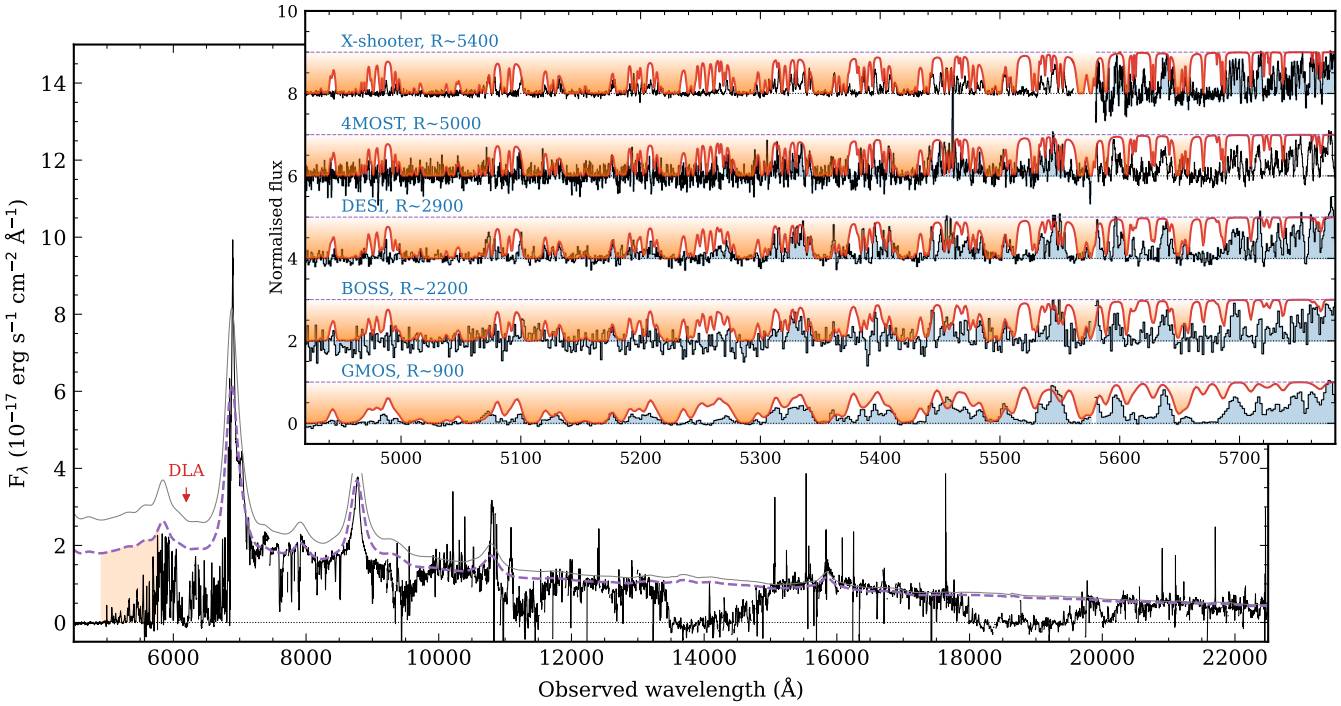

Fig. 1: X-shooter spectrum of the $z = 4.67$ quasar J 0800+3051 (black, smoothed for visual purpose) featuring a DLA at $z = 4.096$ (red arrow). The composite quasar spectrum from Selsing et al. (2016) is shown in grey, and the same composite reddened by A_V=0.06 mag at the DLA redshift is shown as a purple dashed line. The significant decrease in transmission at short wavelengths (orange shaded area) is largely due to strong H_2 absorption lines. The inset shows spectra in this region obtained with different instruments (black line with blue shade), with the synthetic H_2 profile convolved to the corresponding line spread function (red).

very large H I and H_2 columns in the afterglow spectrum of a γ-ray burst by Prochaska et al. (2009). Since long-duration GRBs are linked to the deaths of massive stars, they likely trace dense, star-forming regions within galaxies (Krogager et al. 2024).

In this work, not only does the DLA have the highest molecular fraction directly measured to date at $z > 0$, but it is also found among the very highest redshifts so far (Fig. 2), making its detection surprising by itself. The GMOS survey by Crighton et al. (2015), which includes the object presented in this paper, contains 163 quasars with 45 DLAs at $z > 4$. For comparison, only two intervening absorbers with $\log N(H_2) > 20.5$ have been identified among $\sim 10^4$ DLAs in SDSS at lower redshifts. Moreover, if the H_2 column density distribution, inferred at $z \sim 2.5$ by Krogager & Noterdaeme (2020) from the stacking analysis of Balashev & Noterdaeme (2018), applies at $z \sim 4$, only ~ 0.1 systems with $\log N(H_2) > 20.5$ would be expected in the GMOS survey. The key question is then whether such a difference in detection rate reflects a genuine physical evolution or a combination of selection effects.

From a physical perspective, higher mean gas densities at high redshift, as proposed by Stern et al. (2021), could in principle enhance H_2 formation. In addition, more turbulent neutral gas driven by stronger energy injection from star formation (e.g. Green et al. 2010), accretion (e.g. Elmegreen & Burkert 2010), and mergers (e.g. Bournaud et al. 2011) could promote cold gas and H_2 formation through local density enhancements (see also Colman et al. 2025). These effects may dominate over the opposing influence of lower average metallicities and a stronger ultraviolet radiation field.

On the other hand, our detection may highlight observational selection effects that enter at multiple stages of the detection process. The first step of the detection process involves the identification of the background quasar. In previous quasar surveys, this process is based on a set of complex colour selection criteria and partly builds how the intergalactic medium transmission affects the quasar's spectrum. This colour-based selection is notoriously difficult at $z \sim 2.5-3$ due to the quasar colours crossing the stellar locus (Richards et al. 2002; Krogager et al. 2019). Strong H_2 lines can further absorb a significant fraction of the quasar light bluewards of about 110 nm in the absorber's rest frame, making the quasar identification even more difficult. In the present high-redshift case, the absorber only contributes to the u, g dropout, which is central to the selection of high-redshift quasars and does not alter the colours much, especially since its dust content remains modest. However, in more dust-reddened systems, colour-based selection may become inefficient even at these redshifts. This highlights the importance of complementary selection strategies that are less sensitive to colours (e.g. Krogager et al. 2018, 2023).

Once a spectrum of the quasar has been obtained, the second challenge is the detection of the absorption system itself, which the present system perfectly illustrates by being unnoticed for two decades in public survey data. An efficient strategy to identify H_2 systems is to search for C I absorption, which has been shown to be an excellent tracer of molecular gas (Noterdaeme et al. 2018). Strong transitions are available at 1560 and 1656 Å, i.e. redwards of the Ly-α forest, which facilitates their detection (e.g. Ledoux et al. 2015). Nevertheless, C I absorbers tend to select high-metallicity and dusty absorbers, and they may miss low metallicity molecular systems. Correlation techniques based on H_2 line templates provide a particularly powerful method to recognise the absorption pattern, even when little transmission

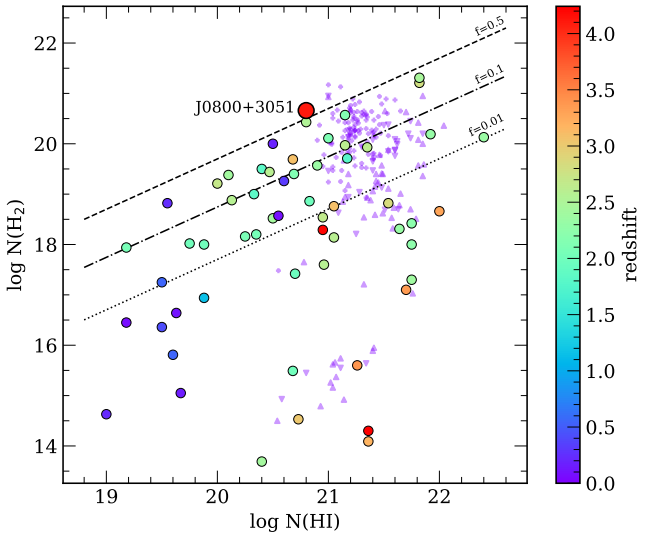

Fig. 2: Column density of molecular vs atomic hydrogen measured from Lyman-Werner and Lyman lines, respectively. Measurements in intervening DLAs (Balashev et al. 2019, and references therein) are represented by circles and coloured by redshift. The $z = 4.1$ system towards J 0800+3051 is highlighted by a larger symbol. Measurements in the Local Group are depicted in purple (Milky Way: plus symbols by Shull et al. 2021; Small and Large Magellanic Clouds: upwards and downwards pointing triangles by Welty et al. 2012). The black lines indicate constant molecular fractions of 0.5, 0.1, and 0.01 (top to bottom).

remains between the H_2 bands. Such methods also have the advantage of being insensitive to the properties of the metals or H I absorption. In fact, the detection presented here arose as a by-product of testing such detection algorithms for H_2 absorption at the quasar redshift (Noterdaeme et al. 2019).

By comparing new observations with archival data, we are now able to examine how the same H_2 absorber manifests itself across surveys with different spectral resolutions, wavelength coverage, and signal-to-noise ratios (see Fig. 1). This provides a rare empirical benchmark for assessing and refining selection and detection algorithms, and it is arguably more informative than mock spectra, as it relies on a real astrophysical system.

Finally, even when a strong H_2 absorber is identified, obtaining robust physical constraints remains challenging. As in the present case, the total column density and kinetic temperature are primarily constrained by the low rotational levels, provided that some transmission remains between absorption bands. The reddest Lyman bands of H_2 are particularly valuable, as they are less affected by mutual blending, whereas lines at shorter wavelengths merge into a quasi-continuum absorption similar to a Lyman limit. As a result, the number of usable transitions decreases at high column densities, making a high S/N and high spectral resolution essential to reliably constraining the rotational populations and inferring physical conditions.

Overall, detecting and characterising extremely strong H_2 absorbers remains challenging. The detection presented in this work may at first glance argue against a significant bias. After all, we did manage to identify this absorption system despite expecting only ~0.1. In turn, this means that we were extremely lucky, the formation of H_2 is more efficient at early cosmic times, or we are missing substantially more H_2 at lower redshifts than currently anticipated. The low dust reddening of this system may have also been crucial to its detection, suggesting that dustier systems are still being missed, which would strengthen these points even more.

Further progress at all redshifts, possibly pushing towards even more extreme and likely rarer systems, will require both more complete quasar selection strategies and further development of efficient H_2 detection techniques. While such absorbers offer a unique window into the dense phases of the neutral gas at high-z, our limited ability to constrain the physical conditions and environment, even when detected, highlights the need for next-generation facilities. Thirty-metre class telescopes equipped with high resolution spectrographs, combined with deep emission observations aimed at detecting the associated galaxies, will be crucial to fully characterising these systems.

Acknowledgements. We thank the referee for useful comments and suggestions. We thank ESO for granting Director's Discretionary Time and Paranal staff for executing our observations. We thank Rodrigo Cuellar for modelling the atmospheric transmission using Molecfit. JKK acknowledges financial support through the French Agence Nationale de la Recherche (ANR) under grant number ANR-24-CE31-7454 (CI-CNM). SB thanks IAP for hospitality and support during a science visit.

References

Balashev, S. A., Klimenko, V. V., Ivanchik, A. V., et al. 2014, MNRAS, 440, 225
Balashev, S. A., Klimenko, V. V., Noterdaeme, P., et al. 2019, MNRAS, 490, 2668
Balashev, S. A. & Noterdaeme, P. 2018, MNRAS, 478, L7
Balashev, S. A., Noterdaeme, P., Rahmani, H., et al. 2017, MNRAS, 470, 2890
Bialy, S. & Sternberg, A. 2016, ApJ, 822, 83
Bournaud, F., Chapon, D., Teyssier, R., et al. 2011, ApJ, 730, 4
Colman, T., Hennebelle, P., Brucy, N., et al. 2025, The Open Journal of Astrophysics, 8, 47517
Crighton, N. H. M., Murphy, M. T., Prochaska, J. X., et al. 2015, MNRAS, 452, 217
Crighton, N. H. M., Prochaska, J. X., Murphy, M. T., et al. 2019, MNRAS, 482, 1456
Dawson, K. S., Schlegel, D. J., Ahn, C. P., et al. 2013, AJ, 145, 10
de Jong, R. S., Agertz, O., Berbel, A. A., et al. 2019, The Messenger, 175, 3
Draine, B. T. 1978, ApJS, 36, 595
Elmegreen, B. G. & Burkert, A. 2010, ApJ, 712, 294
Fall, S. M. & Pei, Y. C. 1993, ApJ, 402, 479
Gordon, K. D., Clayton, G. C., Misselt, K. A., Landolt, A. U., & Wolff, M. J. 2003, ApJ, 594, 279
Green, A. W., Glazebrook, K., McGregor, P. J., et al. 2010, Nature, 467, 684
Krogager, J.-K., De Cia, A., Heintz, K. E., et al. 2024, MNRAS, 535, 561
Krogager, J.-K., Fynbo, J. P. U., Møller, P., et al. 2019, MNRAS, 486, 4377
Krogager, J.-K., Gupta, N., Noterdaeme, P., et al. 2018, ApJS, 235, 10
Krogager, J.-K., Leighly, K. M., Fynbo, J. P. U., et al. 2023, The Messenger, 190, 38
Krogager, J.-K., Møller, P., Christensen, L. B., et al. 2020, MNRAS, 495, 3014
Krogager, J.-K. & Noterdaeme, P. 2020, A&A, 644, L6
Lacour, S., Ziskin, V., Hébrard, G., et al. 2005, ApJ, 627, 251
Ledoux, C., Noterdaeme, P., Petitjean, P., & Srianand, R. 2015, A&A, 580, A8
Ledoux, C., Petitjean, P., Fynbo, J. P. U., Møller, P., & Srianand, R. 2006a, A&A, 457, 71
Ledoux, C., Petitjean, P., & Srianand, R. 2006b, ApJ, 640, L25
Noterdaeme, P., Balashev, S., Berg, T., et al. 2026, A&A, 707, A66
Noterdaeme, P., Balashev, S., Krogager, J.-K., et al. 2019, A&A, 627, A32
Noterdaeme, P., Krogager, J.-K., Balashev, S., et al. 2017, A&A, 597, A82
Noterdaeme, P., Ledoux, C., Zou, S., et al. 2018, A&A, 612, A58
Noterdaeme, P., Petitjean, P., Carithers, W. C., et al. 2012, A&A, 547, L1
Noterdaeme, P., Petitjean, P., Pâris, I., et al. 2014, A&A, 566, A24
Noterdaeme, P., Petitjean, P., & Srianand, R. 2015, A&A, 578, L5
Prochaska, J. X., Herbert-Fort, S., & Wolfe, A. M. 2005, ApJ, 635, 123
Prochaska, J. X., Sheffer, Y., Perley, D. A., et al. 2009, ApJ, 691, L27
Ranjan, A., Noterdaeme, P., Krogager, J. K., et al. 2018, A&A, 618, A184
Richards, G. T., Fan, X., Newberg, H. J., et al. 2002, AJ, 123, 2945
Schneider, D. P., Hall, P. B., Richards, G. T., et al. 2005, AJ, 130, 367
Selsing, J., Fynbo, J. P. U., Christensen, L., & Krogager, J.-K. 2016, A&A, 585, A87
Shull, J. M., Danforth, C. W., & Anderson, K. L. 2021, ApJ, 911, 55
Smette, A., Sana, H., Noll, S., et al. 2015, A&A, 576, A77
Stern, J., Sternberg, A., Faucher-Giguère, C.-A., et al. 2021, MNRAS, 507, 2869
Trakhtenbrot, B., Netzer, H., Lira, P., & Shemmer, O. 2011, ApJ, 730, 7
Vernet, J., Dekker, H., D'Odorico, S., et al. 2011, A&A, 536, A105
Welty, D. E., Xue, R., & Wong, T. 2012, ApJ, 745, 173
Worseck, G., Prochaska, J. X., O'Meara, J. M., et al. 2014, MNRAS, 445, 1745
York, D. G., Adelman, J., Anderson, Jr., J. E., et al. 2000, AJ, 120, 1579

Appendix A: Notes on absorption modelling and column density measurements

Appendix A.1: Atomic hydrogen

The total atomic hydrogen column density in the DLA was constrained from the Ly-α line. Because of contaminating absorption from H I forest in the wings, the fit was constrained using the local transmission peaks, yielding $\log N(\mathrm{H\,I}) = 20.8 \pm 0.1$, see Fig. A.1. This value matches the estimate based on SDSS data by Prochaska et al. (2005) but is lower than that from GMOS data ($\log N(\mathrm{H\,I}) = 21.05$; Crighton et al. 2015) probably due to contamination by the Ly-α forest unrecognised at the lower achieved spectral resolution.

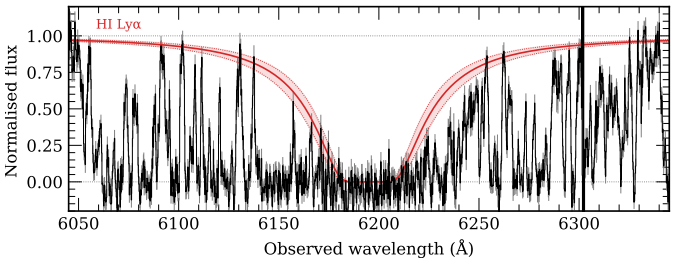

Fig. A.1: Damped H I Ly-α profile. The data is shown in black with uncertainties in grey. The model with $\log N(\mathrm{H\,I}) = 20.8$ is shown in red with 0.1 dex range shown by the shaded area.

Appendix A.2: Low-ionisation metal lines

Metals absorption lines from low-ionisation species (Si II, Fe II, and Al II) are detected in multiple components spanning approximately 500 km s^{-1}. Owing to the high redshift, only Si IIλ1526, Si IIλ1808, Fe IIλ1608, and Al IIλ1670 fall redwards of the Ly-α forest. Among these, Si IIλ1808 and Fe IIλ1608 are weak and partially blended with telluric absorption, while the other two transitions contain components in the intermediate regime. Consequently, although a simultaneous fit assuming common redshift and Doppler parameter (z, b) across species provides a visually good fit to the data, the column densities in the individual components could be degenerate. The total column densities, provided in Table A.1, should however be more robust.

Appendix A.3: Neutral carbon

Neutral carbon absorption lines are clearly detected at the velocity of the H_2 component along with the three fine-structure levels. A slight asymmetry suggests the presence of two components, which we used to model the λ1560 and 1656 lines that are located outside the Ly-α forest, see Fig. A.3. Intrinsic saturation leads to large uncertainties on their column densities as reported in Table A.1.

Appendix A.4: Modelling the H_2 absorption profile

Because of the strong blending among the H_2 lines, further affected by contamination from the H I forest, constraining the H_2 column densities is challenging. We found that different modelling choices and assumptions can yield significantly different column densities in the high rotational levels while providing comparably good fits to the data. We therefore adopted a conservative approach and report the full range of column densities

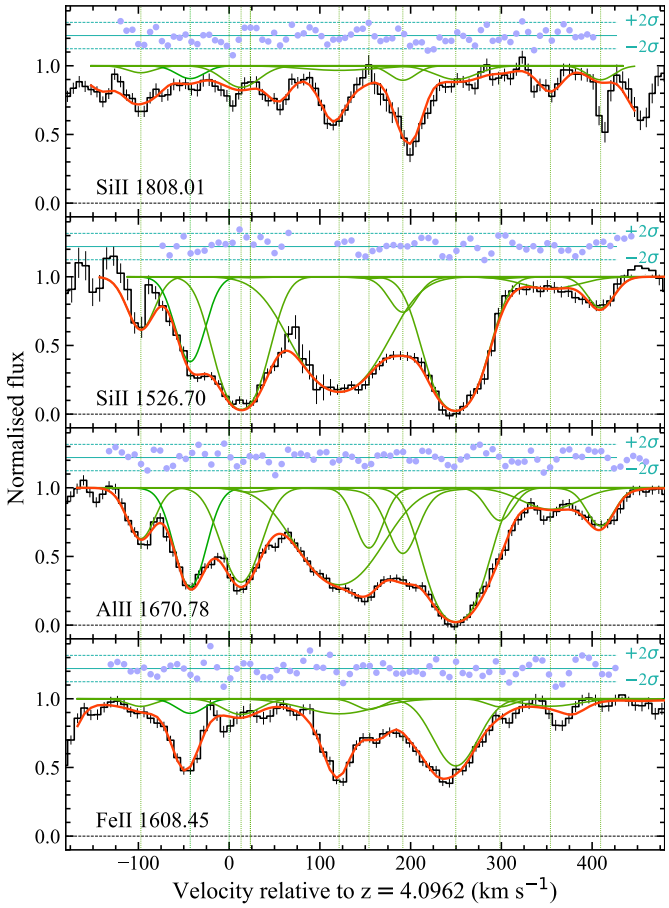

Fig. A.2: Low-ionisation metal absorption lines. The data is shown in black with the overall absorption model in red. Contribution from individual components is shown in green and that from telluric lines depicted as purple shaded area. Note that two regions in the Si IIλ1526 profile at about −100 and +100 km s^{-1} are affected by sky emission line residuals and not used to constrain the fit. Residuals are shown in the top panels.

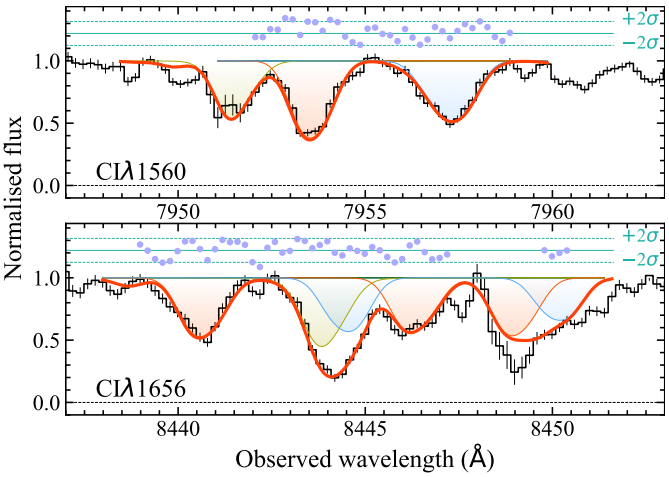

Fig. A.3: C I absorption lines. The data are shown in black with the overall absorption model in red. Contribution from the different fine-structure levels are shown by green (J=0), orange (J=1) and blue (J=2) shaded areas while that of telluric lines is shown in purple.

Table A.1: Total column densities measured in the $z_{\rm abs} = 4.1$ DLA towards J 0800+3051.

Species	$\log N/{\rm cm}^{-2}$
H I	20.8 ± 0.1
Si II	$15.66^{+0.34}_{-0.10}$
Fe II	14.50 ± 0.03
Al II	$15.09^{+0.15}_{-0.13}$
C I,J=0	$16.5^{+0.4}_{-0.8}$
C I,J=1	$15.2^{+0.8}_{-0.3}$
C I,J=2	$14.58^{+0.08}_{-0.08}$
H_2,J=0	20.18 ± 0.10
H_2,J=1	20.37 ± 0.03
H_2,J=2	19.50 ± 0.20
H_2,J=3	19.46 ± 0.15
H_2,J=4	18.2-19.2
H_2,J=5	18.0-19.2
H_2,J=6	16.6-18.8
H_2,J=7	16.1-18.2
H_2,J=8	15.1-15.9
H_2,J=9	15.1-16.0
total H_2	20.66 ± 0.04 [†]

Notes. [(†)] Obtained from summing the central values across levels. The quoted uncertainty represents the formal propagation of the model ranges, treating them as 1 σ standard errors.

obtained from a variety of models: (i) a single-component H_2 model with a common Doppler parameter for all rotational levels; (ii) the same model allowing the Doppler parameter to increase with rotational level, as sometimes observed in the literature (e.g. Lacour et al. 2005); and (iii) two-component models, motivated by a possible asymmetry in the high-J lines and in the C I profiles, with either tied or level-dependent Doppler parameters. We also considered the cumulative absorption from the H I forest as a pseudo-continuum variation. Since the dense and heavily blended H I lines make the detailed transmission difficult to model, their net effect was approximated by a linear correction to the unabsorbed quasar continuum. The inferred column densities are highly consistent across models up to $J = 3$, for which we give the central point with range as uncertainty but diverge substantially for $J \geq 4$, for which we provide a range only in Table A.1. The contribution of lines from different rotational levels to the overall absorption model is highlighted in Fig. A.4.

Appendix A.5: Additional high column density H I *systems*

We also identified a strong sub-DLA at $z = 3.669$ with $\log N({\rm H\,I}) \simeq 20$, accompanied by low-ionisation metal absorption lines (Si IIλ1526, Al IIλ1670). In addition, we derived a slightly revised absorption redshift ($z = 4.387$ instead of $z = 4.386$) based on the Si IV and C IV features observed in the X-shooter data for the Lyman-limit system reported by Crighton et al. (2019). These systems are included in the overall absorption model shown in Fig. A.4.

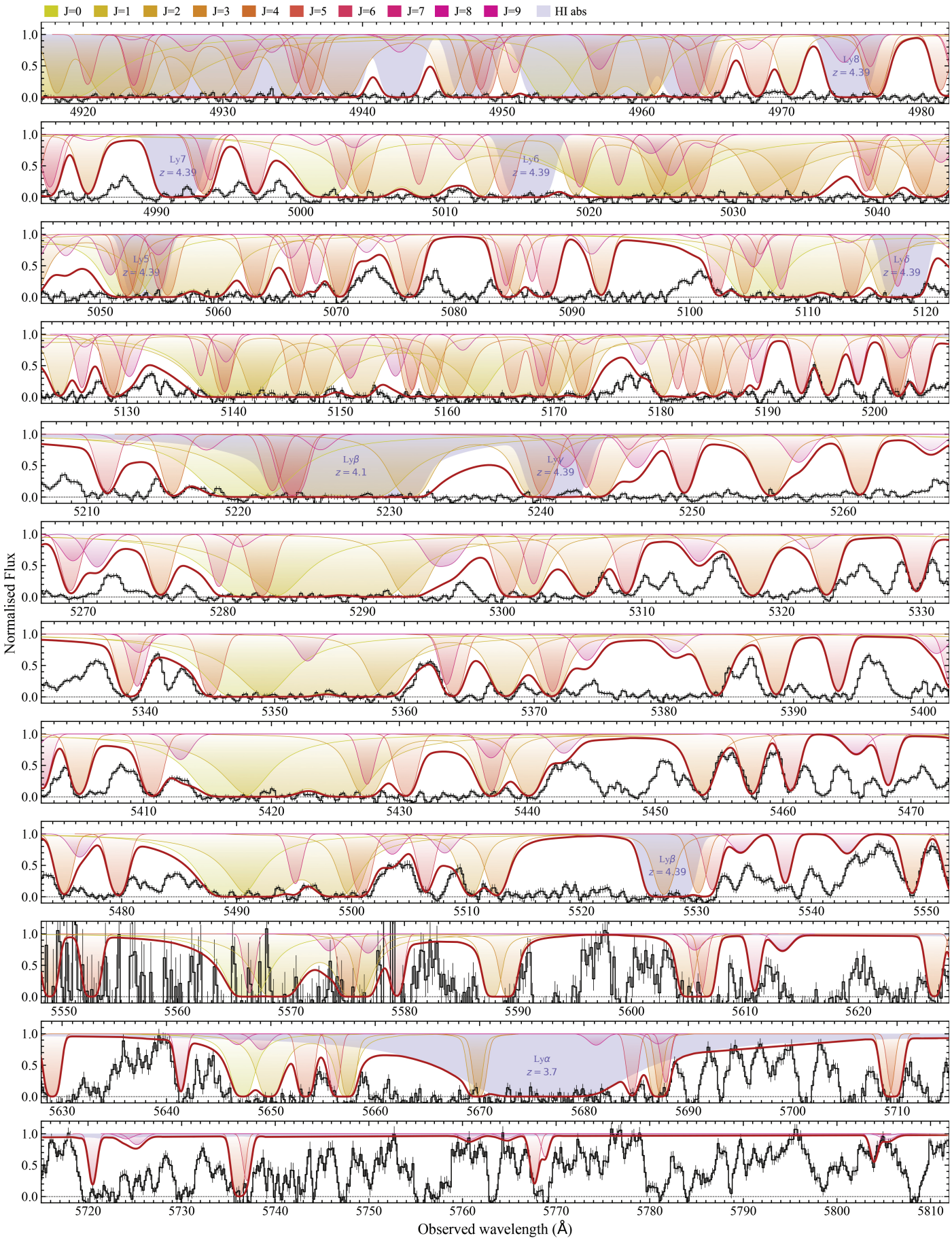

Fig. A.4: Portion of the normalised X-shooter spectrum (black) with the overall fitted absorption model (red line). The contribution from low to high rotational levels of H_2 at $z = 4.0962$ is shown by the yellow to red gradient fill (see top legend). Blue areas represent H I absorption from the $z = 4.096$ DLA and the sub-DLAs at $z = 3.669$ and $z = 4.387$.